Article:
Yun, X., Zhu, Y. and Gardner, L. (2023) Experimental investigation of steel frames made of hybrid steel welded I-sections. ce/papers, 6 (3-4). pp. 1668-1673. ISSN 2509-7075

https://doi.org/10.1002/cepa.2518

Experimental investigation of steel frames made of hybrid steel welded I-sections

Xiang Yun[1] | Yufei Zhu[2] | Leroy Gardner[2]

1 Introduction

High strength steels (HSS) with nominal yield strengths equal to or greater than 460 MPa are gaining growing popularity in modern construction practice worldwide, owing largely to their intrinsic high strength-to-weight ratio and potential for reductions in steel consumption and CO_2 emissions in the construction sector. HSS I-sections are generally fabricated from welded plates, where two flange plates are welded to a single web plate. Compared to homogenous HSS welded I-sections (i.e. the flange and web plates are made of the same HSS grade), hybrid steel welded I-sections (i.e. the flange plates are made of a higher steel grade than the web plate) can lead to more economical solutions [1] because of the use of a less expensive lower steel grade for the web plate, which contributes only a modest amount to the bending rigidity and resistance of structural elements, than for the flange plates. To date, hybrid steel welded I-section structural members have gained increased interest among researchers, and a considerable number of studies have been performed to investigate the structural performance of hybrid steel welded I-section columns [2,3] and beams [4]. However, there have been no experimental investigations into the performance of hybrid steel welded I-sections at the structural system level, which, to a certain extent, hinders the development of structural design rules for hybrid steel welded I-sections and thereby inhibits their wide application in the construction industry.

Towards addressing this knowledge gap, experimental studies on four full-scale, single-bay, single-storey frames made of hybrid steel welded I-sections (i.e. S355 steel for web and S690 steel for flanges) have been carried out. Out-of-plane restraints were provided to all the tested frame specimens to effectively prevent out-of-plane instability which is out of the scope of the present study. The experimental program featured the use of digital image correlation (DIC) to obtain full-field displacement/strain measurements of the frame specimens, providing thorough information on their structural performance. The test setup and loading procedures, as well as the key experimental results, including the failure modes, ultimate collapse loads and load-displacement histories, are presented in this paper. The obtained experimental results can serve as benchmark data for the validation of high-fidelity numerical models and the development of suitable design methods for steel frames made of hybrid steel welded I-section members.

2 Experimental program

2.1 Tensile coupon tests

The stress-strain characteristics of the investigated S355

and S690 steels were determined by means of tensile coupon tests. The tensile coupons were cut from the same batch of plates as used for the fabrication of the frame specimens. Specifically, a total of four longitudinal tensile coupons (two S355 steel coupons and two S690 steel coupons) were extracted from corresponding 8 mm-thick plates along the rolling direction. All coupons were tested under uniaxial monotonic loading by means of displacement control using a 250 kN hydraulic testing machine, with the displacement rate of 0.05 mm/min before yielding followed by a higher rate of 0.5 mm/min for the post-yield range. The measured engineering stress-strain curves are shown in Figure 1, while the key average material properties, including the Young's modulus E, the yield strength f_y, the ultimate tensile strength f_u, the strain hardening strain ε_{sh} and the ultimate strain ε_u corresponding to f_u are summarised in Table 1.

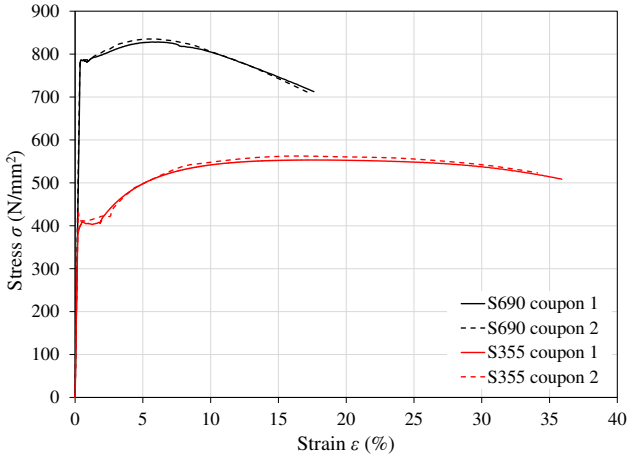

Figure 1 Engineering stress-strain curves for the investigated S355 and S690 steels.

Table 1 Average material properties of the investigated S355 and S690 steels.

Steel grade	E N/mm²	f_y N/mm²	f_u N/mm²	ε_{sh} %	ε_u %
S355	198500	404.1	553.5	1.89	17.22
S690	212000	782.5	828.4	0.96	6.17

2.2 Frame specimens

A total of four two-dimensional, full-scale, single-bay, single-storey frames was tested; the configuration of the test frame specimens is shown in Figure 2. The span of the frames (i.e. the distance between the column centrelines) was 3.168 m and the height of the frames (i.e. from the base of the columns to the centreline of the beam) was 2 m. For each of the four tested frames, the same hybrid steel welded I-section with quenched and tempered S690 steel flanges and an S355 steel web was employed for both the columns and the beam. Each frame specimen was labelled by a unique identifier, e.g. HYB-I-80×136×8×8-V, where "HYB-I" denotes a hybrid welded I-section which is followed by the nominal dimensions (flange width B × outer section depth H × flange thickness t_f × web thickness t_w) of the hybrid welded I-section of 80×136×8×8. The notation after the cross-section identifier refers to the loading condition of the frame specimen, where "V" indicates that the frame is subjected to pure vertical load, 'H' indicates that the frame is subjected to pure horizontal load, and "V&H-1" and "V&H-2" indicate that the frame is subjected to combined vertical and horizontal loads, with different vertical-to-horizontal load ratios. The average measured geometric dimensions of the cross-section of each frame specimen are presented in Table 2, where t_{weld} is the weld leg length.

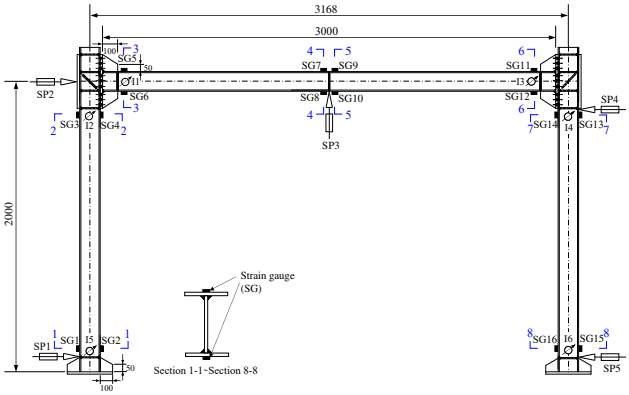

Figure 2 Configuration of frame specimens and instrumentation, including strain gauges (SG), string potentiometers (SP) and inclinometers (I). Dimensions are shown in mm.

Table 2 Average measured geometric dimensions of frame specimens

Frame label	B mm	H mm	t_f mm	t_w mm	t_{weld} mm
HYB-I-80×136×8×8-V	79.4	136.9	8.29	8.26	5.66
HYB-I-80×136×8×8-H	79.2	136.6	8.34	8.24	5.37
HYB-I-80×136×8×8-V&H-1	78.8	136.8	8.44	8.35	4.90
HYB-I-80×136×8×8-V&H-2	79.6	136.6	8.48	8.36	5.33

The beam-to-column connections of the frame specimens comprised a 16-mm thick beam end plate, made of S690 steel, which was fillet welded to the beam end and bolted to the column flange using eighteen preloaded high strength M16 bolts. The beam end plate has a greater width than that of its connected column, thereby enabling the beam-to-column connection to be further strengthened by means of bolting the beam end plate to a strengthening plate attached to the outer side of the column flange using ten preloaded high strength M20 bolts, as illustrated in Figure 3. Each of the M20 bolts was housed within a steel tube, positioned between the beam end plate and the stiffening plate (see Figure 3), to prevent the inward bending of the two plates due to the preload in the M20 bolts.

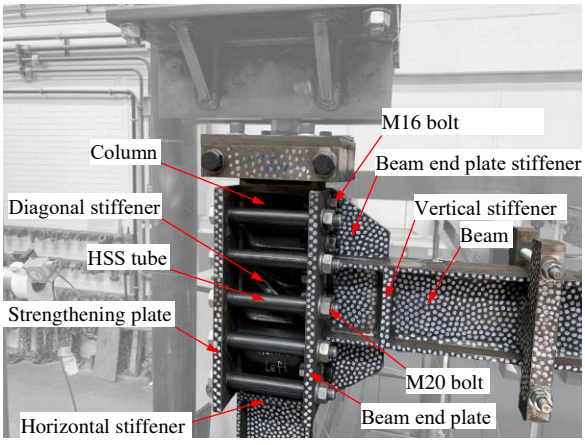

Figure 3 Photo of beam-to-column connection.

A series of stiffeners were cut from 16 mm thick S690 steel plates and welded onto the frame panel zones and beam end plates to increase the strength and stiffness of the connections. Note that the presence of the beam end plate stiffeners also had the effect of shifting the plastic hinge locations away from the beam ends to the beam sections where the stiffeners terminated; the column end plate stiffeners had the same effect.

3 Frame test setup and instrumentation

The schematic solidworks model of the frame test setup is shown in Figure 4. The test rig contained three main hydraulic actuators, four external support frames and top and bottom loading beams, as illustrated in Figure 4. A similar test setup has been successfully employed for stainless steel frames [5].

3.1 Loading conditions

Different loading conditions were applied to the four frame specimens, with one subjected to vertical load V only applied at the mid-span of the beam, one subjected to horizontal load H only applied to the bottom loading beam and the other two subjected to different combinations of the two (V and H). For the frames subjected to combined loading, the vertical load V_{test} was first applied at the mid-span of the beam until the pre-determined load was reached (i.e. 130 kN and 170 kN for HYB-I-80×136×8×8-V&H-1 and HYB-I-80×136×8×8-V&H-2 respectively). The vertical load V_{test} was then held constant while the horizontal load H_{test} was applied at the column base through the bottom loading beam until either collapse of the frame or excessive deformation occurred. For all the frame tests, the vertical load was applied under load control at a slow rate of approximately 5 kN/min, while the horizontal load was introduced under displacement control at approximately 2 mm/min. The vertical load was applied using two 232 kN (25 tonne) hydraulic actuators, which were mounted on the bottom flange of the top loading beam, in alignment with the mid-span of the beam of the frame specimen. The top loading beam was a 250 × 250 × 8 mm cold-formed S700 steel square hollow section (SHS), which was fixed to the vertical support frame, as shown in Figure 4. The vertical load was measured using a calibrated load cell positioned under the vertical hydraulic actuators and applied through a steel roller. A pair of stiffeners was welded to the frame specimen at the vertical loading point to prevent web crippling due to the concentrated vertical load.

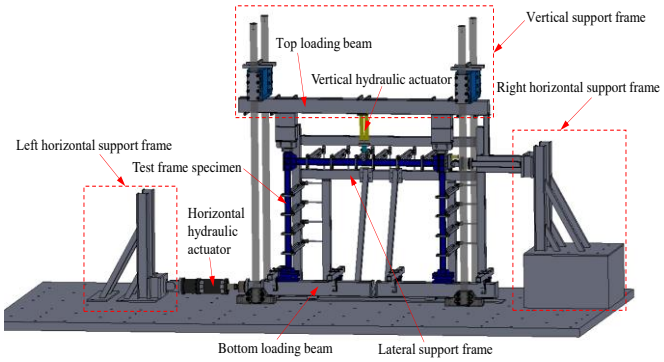

Figure 4 Schematic solidworks model of frame test setup.

The horizontal load was applied to the bottom loading beam by a 250 kN hydraulic actuator, which was mounted on the left horizontal support frame, as illustrated in Figure 4. The frame specimens were fixed to the bottom loading beam, which was seated on several greased roller bearings, allowing the frames to move in-plane with minimal friction. The frame specimens were horizontally restrained at the top of the right-hand column by a horizontal support. The horizontal support included a manual hydraulic pump, a bearing plate and a set of steel rollers, as illustrated in Figure 5. The manual hydraulic pump was fixed to the bearing plate, and the pump head (featuring the roller bearings) was attached to the surface of the strengthening plate prior to testing, as shown in Figure 5(a). For the frame specimens that were loaded horizontally, the manual hydraulic pump was used to adjust the position of the bearing plate such that it remained vertical during testing, as shown in Figure 5(b); this ensured that the reaction remained horizontal, despite the rotation of the right-hand beam-to-column connection. The load provided by the manual hydraulic pump was increased as the horizontal load increased, approximately to half of the applied horizontal load. The horizontal support provided a "hinge-like" boundary condition at the top of the right-hand column. The horizontal load was applied at the base level, allowing the vertical actuator to remain stationary during testing, rather than requiring it to move laterally with the frame. This loading configuration is statically equivalent to applying the horizontal load at the right-hand beam-to-column connection and restraining lateral movements at the column bases. Note that the bottom loading beam was of the same cross-section profile as the top loading beam, but was filled with concrete to prevent any local failure of the tube due to the concentrated loading.

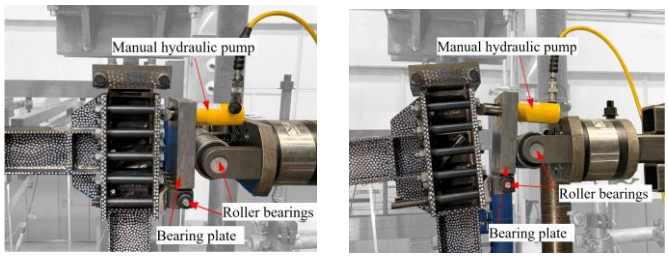

(a) (b)

Figure 5 Horizontal support (a) prior to testing; (b) during testing.

3.2 Lateral restraints

A bespoke restraint system was designed to prevent out-of-plane instability of the test frames without inducing any undesirable in-plane restraint. The restraint system comprised a total of 14 out-of-plane lateral restraints, among which 6 were used to provide lateral restraint to the beam of the test frames and 4 provided lateral restraint to each column, as shown in Figure 4. A detailed description of the lateral restraint system and the approach of adjusting the position of the restraints so that they were moved along with the deformations of the frame specimens at the corresponding locations can be found in [6].

3.3 Instrumentation

Electrical resistance strain gauges were mounted on the top and bottom flanges at selected locations on the frame specimens to estimate bending moments and monitor the strain development histories during testing. As indicated

in Figure 2, a total of eight beam and column sections (Sections 1-1 to 8-8 in Figure 2) were monitored, located adjacent to (i.e. at a distance of 50 mm from the corresponding stiffened section) the base of each frame column, the beam-to-column connections and the mid-span of the beam, covering the most highly stressed regions of the frames under the different loading scenarios. String potentiometers (SP) were used to measure the in-plane vertical deflections at the mid-span of the beam (see SP3 in Figure 2) and the in-plane horizontal deflections at the base and top of each column (see SP1, SP2, SP4 and SP5 in Figure 2). Note that SP4 was placed below the strengthening plate of the right-hand beam-to-column connection for the frame specimens subjected to horizontal loading to avoid conflict with the horizontal restraint system. In addition, a total of six inclinometers (I) was employed on each frame, positioned close to the beam-to-column connections and the column base connections to measure the rotation of the connections and to evaluate their rotational stiffnesses. The test outputs, including the applied loads and displacements from the hydraulic actuators, as well as the readings from the strain gauges, string potentiometers and inclinometers, were continuously monitored and recorded at 1-s intervals using the data acquisition system DATASCAN.

3.4 Digital image correlation (DIC)

Digital Image Correlation (DIC) was also employed to provide more comprehensive displacement and strain measurements. Compared with conventional instrumentation which is commonly used to monitor deformations at key discrete locations, DIC enables full-field measurements to be captured, making it ideal for use in structural testing. A four-camera LaVision DIC system was used for the image acquisition, as shown in Figure 6, among which two cameras with 8 mm focal length lenses (Cameras 1 and 2 in Figure 6) were used to monitor the deformation fields of the full frame specimens, while the other two cameras (Cameras 3 and 4 in Figure 6), which were equipped with longer focal length lenses of 35 mm to ensure sufficient resolution, were employed to record the surface strain field at the most highly stressed region (i.e. the region where the first plastic hinge formed), which could be either at the base of one column or at the mid-span of the beam depending on the loading scenario, throughout testing. Prior to testing, the front surface of all frame specimens was sprayed with a thin layer of black paint, on top of which different random white speckle patterns were drawn in order to achieve an average speckle size of 3–5 pixels in the acquired images from the two pairs of cameras. Consequently, a fine speckle pattern was applied to the most highly stressed region of each frame while a relatively coarse speckle pattern was used elsewhere, as illustrated in Figure 6. The output signals from the horizontal and vertical hydraulic actuators were fed into the DIC system through an analogue-to-digital converter, while images were captured at 2-s intervals and processed using the DaVis version 8.4.0 imaging software (LaVision 2017 [7]). The measurements from the strain gauges, string potentiometers and inclinometers, as described in the previous subsection, were used to corroborate the DIC measurements at key locations.

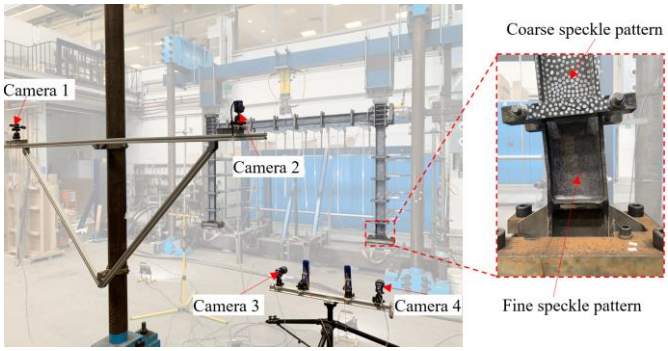

Figure 6 DIC setup and speckle patterns for frame tests.

4 Test observations and discussion

4.1 Ultimate collapse loads

Table 3 summarises the maximum vertical loads (or the predetermined vertical loads for the frame specimens subjected to combined loading) $V_{test,max}$ and the corresponding vertical displacements at the mid-span of the beam of the frame specimens δ_{mid}, as well as the maximum horizontal loads $H_{test,max}$ and the corresponding horizontal displacements at the column bases δ_{base}.

Table 3 Summary of maximum applied loads and the corresponding displacements for frame test specimens.

Frame label	Vertical loading step		Horizontal loading step	
	$V_{test,max}$ kN	δ_{mid} mm	$H_{test,max}$ kN	δ_{base} mm
HYB-I-80×136×8×8-V	227.0	155.2	-	-
HYB-I-80×136×8×8-H	-	-	191.9	205.3
HYB-I-80×136×8×8-V&H-1	131.1	20.0	165.3	194.9
HYB-I-80×136×8×8-V&H-2	170.1	39.0	138.0	158.1

4.2 Failure modes

The failure mode of the tested frame specimen subjected to vertical load only (i.e. HYB-I-80×136×8×8-V) featured a beam collapse mechanism in which significant plastic deformations were observed at the mid-span of the beam (i.e. the position where the vertical load was applied) and adjacent to the beam-to-column connections, as displayed in Figure 7(a). The maximum measured tensile strain occurred at the bottom flange adjacent to the mid-span of the beam (as obtained from the strain gauge readings of either SG8 or SG10, as illustrated in Figure 2), reaching a maximum value of 4.3% which is far in excess of the yield strain of 0.37% measured from the tensile coupon tests. Large tensile strains were also measured at the outer flanges of the columns adjacent to the beam-to-column connections, with maximum tensile strains attained up to 2.6% and 2.0% at Section 2-2 (i.e. SG3) and Section 7–7 (i.e. SG13), respectively.

The test specimen subjected to horizontal load only (i.e. HYB-I-80×136×8×8-H) failed due to material yielding, the spread of plasticity and the formation of a sway plastic collapse mechanism, as shown in Figure 7(b) and discussed below. The maximum tensile strains were recorded from the strain gauges located adjacent to the base of the

columns (i.e. SG2 at Section 1-1 and SG15 at Section 8–8, as illustrated in Figure 2), with the maximum tensile strain measured from SG15 being slightly larger than that from SG2, reaching approximately 3.9%. The measured maximum tensile strains at the locations adjacent to the beam-to-column connections were also beyond the measured yield strain of 0.37%, indicating yielding had occurred at these positions prior to failure. The attainment of high strains adjacent to the column bases and to the beam-to-column connections signifies the development of plastic hinges and the formation of the sway plastic collapse mechanism.

(a)

(b)

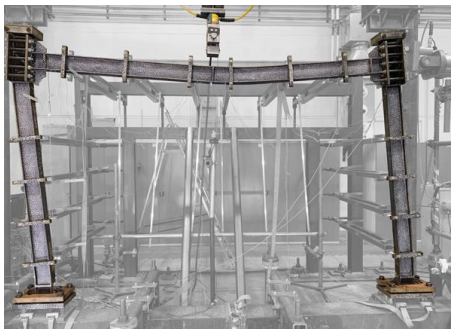

(c)

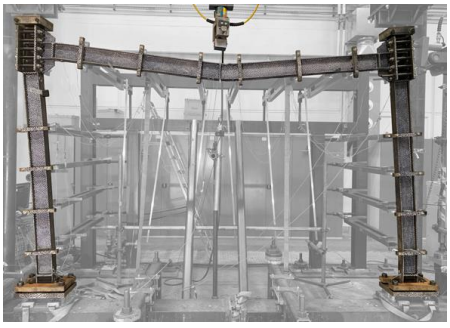

(d)

Figure 7 Failure modes of tested frame specimens (a) HYB-I-80×136×8×8-V, (b) HYB-I-80×136×8×8-H, (c) HYB-I-80×136×8×8-V&H-1 and (d) HYB-I-80×136×8×8-V&H-2.

The failure modes of HYB-I-80×136×8×8-V&H-1 and HYB-I-80×136×8×8-V&H-2 were characterized by a combined beam and sway plastic collapse mechanism, as shown in Figures 7(c) and 7(d), but with different hinge formation sequences owing to the different loading conditions. The tensile strain at the bottom flange adjacent to the mid-span of the beam for frame specimen HYB-I-80×136×8×8-V&H-1 (taken as the average strain from the pair of SG8 and SG10, illustrated in Figure 2) reached 0.30% when the predetermined vertical load $V_{test,max}$, as given in Table 3, was applied, which was lower than the measured yield strain of 0.37% indicating that the stresses within the section at the mid-span of the beam remained in the elastic range prior to the introduction of the horizontal load. However, for the other frame specimen HYB-I-80×136×8×8-V&H-2, first yield occurred at the mid-span of the beam prior to the horizontal load being applied, with the maximum average tensile strains (from the pair of SG8 and SG10) being 0.63% when the corresponding predetermined vertical load $V_{test,max}$ was reached. For the two frame specimens subjected to combined loading, different degrees of plastic deformation occurred at the mid-span of the beam, the column bases and adjacent to the left-hand beam-to-column connection, while the sections adjacent to the right-hand beam-to-column connection remained elastic, since relatively low levels of bending moment and compression were experienced here in the combined load cases. The observed order of yielding was generally consistent with the anticipated sequence of plastic hinges determined from a first order plastic analysis.

4.3 Load versus displacement curves

The relationships between the vertical applied load and the vertical displacement at the mid-span of the beam for the frame specimen subjected to vertical load only (i.e. HYB-I-80×136×8×8-V) is plotted in Figure 8.

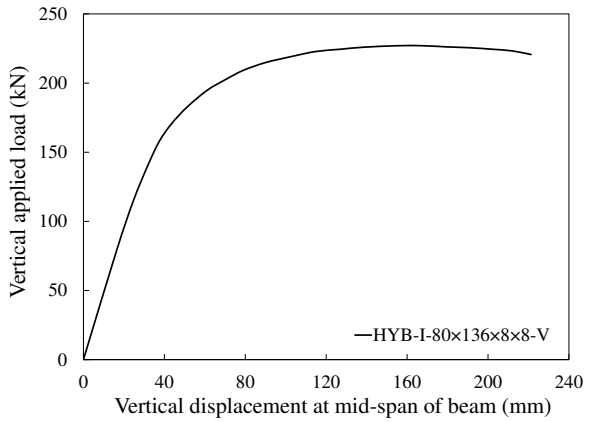

Figure 8 Vertical load versus mid-span displacement curve for HYB-I-80×136×8×8-V.

Figure 9 shows the response of the frame specimen (i.e. HYB-I-80×136×8×8-H) subjected to horizontal load only in terms of the horizontal applied load versus the horizontal displacement at the column bases.

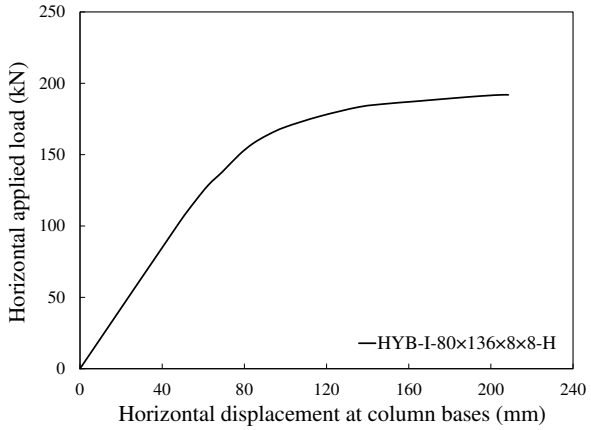

Figure 9 Horizontal load versus horizontal displacement curve for HYB-I-80×136×8×8-H.

Both the vertical and horizontal responses of the frame specimens subjected to combined vertical and horizontal loads (i.e. HYB-I-80×136×8×8-V&H-1 and HYB-I-80×136×8×8-V&H-2) are plotted in Figure 10. The load–displacement curves for the frame specimens subjected to vertical load or horizontal load only are also plotted in Figure 10 for comparison purposes. As shown in Figure 10, during the vertical loading step, which was always first, the vertical applied load versus the vertical displacement curves for the frame specimens subjected to combined loading conditions follow those of the corresponding frame specimens under vertical load only. During the horizontal loading step, the vertical load remained constant while the vertical displacement at the mid-span of the beam grew as the horizontal load increased, as shown in Figure 10. The presence of the vertical load for the frame specimens subjected to combined loading conditions led to a degradation of both strength and stiffness compared to those of the corresponding frame specimens subjected to horizontal load only, with the larger vertical load (i.e. HYB-I-80×136×8×8-V&H-2) resulting in greater loss of resistance and stiffness, as shown in Figure 10.

5 Conclusions

A comprehensive experimental investigation into the structural behaviour of steel frames made of hybrid steel welded I-section (i.e. S355 steel for web and S690 steel for flanges) members has been presented in this paper. A total of four two-dimensional, single bay, single storey, unbraced rectangular hybrid steel frames were tested. The experimental setup, including the implementation of different loading schemes and the use of a bespoke restraint system to prevent out-of-plane instability has been described. The ultimate collapse loads, load-deformation characteristics and failure modes of the frames have been presented and discussed. The experimental results indicated that, despite the lower ductility and strain hardening of HSS relative to normal strength steels, hybrid steel frames with stocky cross-sections have the ability to form plastic hinges and achieve a considerable amount of inelastic moment redistribution. The available ductility and potential for plastic design of hybrid steel structures has been highlighted and will be examined further in future work.

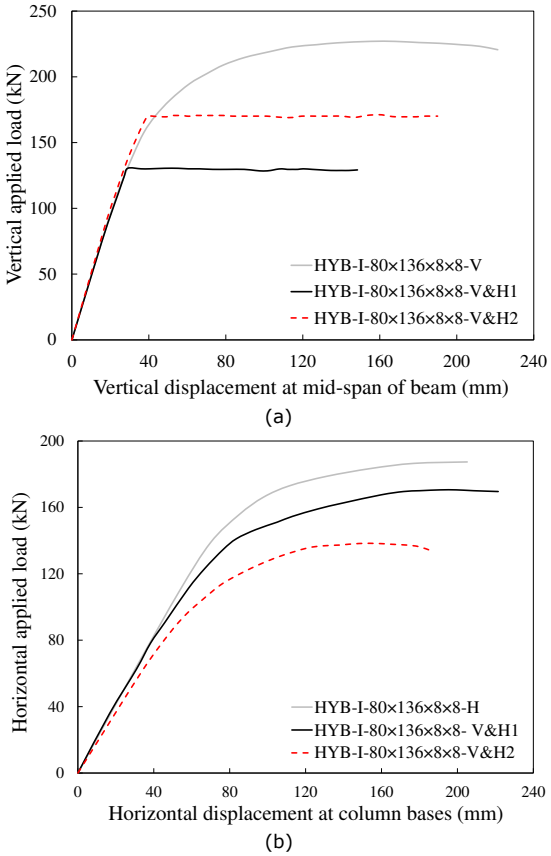

Figure 10 Load-displacement curves for frame specimens subjected to combined vertical and horizontal loads (a) vertical load versus mid-span displacement curves and (b) horizontal load versus horizontal displacement curves.

References

[1] Veljkovic, M.; Johansson, B. (2004) *Design of hybrid steel girders*. Journal of Constructional Steel Research 60(3-5), 535-547.

[2] Yun, X.; Zhu, Y.; Meng, X; Gardner, L. (2023) *Welded steel I-section columns: residual stresses, testing, simulation and design*. Engineering structures, 282, 115631.

[3] Chen, S.; Liu, J.Z.; Chan, T.M. (2023) *Investigations into the local buckling and post-buckling behaviour of fixed-ended hybrid I-section stub columns with slender web*. Thin-Walled Structures, 184, 110174.

[4] Zhu, Y.; Yun, X.; Gardner, L. (2023) *Behaviour and design of high strength steel homogeneous and hybrid welded I-section beams*. Engineering Structures 275, 115275.

[5] Arrayago, I.; González-de-León, I.; Real, E.; Mirambell, E. (2020) *Tests on stainless steel frames. Part I: Preliminary tests and experimental set-up.* Thin-Walled Structures 157, 107005.

[6] Yun, X.; Zhu, Y.; Wang, Z.; Gardner, L. (2022) *Benchmark tests on high strength steel frames*. Engineering Structures 258, 114108.

[7] LaVision. DaVis imaging software. Ypsilanti, MI: LaVision, 2007.